Appl. Phys. A 75, 17–23 (2002) / Digital Object Identifier (DOI) 10.1007/s003390101051

Applied Physics A
Materials
Science & Processing

A kinetic Monte Carlo investigation of island nucleation and growth in thin-film epitaxy in the presence of substrate-mediated interactions

K.A. Fichthorn[1,*], **M.L. Merrick**[1], **M. Scheffler**[2]

[1] Department of Chemical Engineering, The Pennsylvania State University, University Park, PA 16802, USA
[2] Fritz-Haber-Institut der Max-Planck-Gesellschaft, Faradayweg 4-6, 14195 Berlin, Germany

Received: 30 April 2001/Accepted: 23 July 2001/Published online: 3 April 2002 –

Abstract. Island nucleation and growth during thin-film epitaxy is typically described using mean-field rate equations, which can be solved to predict the density of stable islands as a function of the deposition rate and the diffusivity of an isolated adatom. Recent theoretical and experimental studies indicate that medium- and long-range interactions between adatoms may change the simple picture that nucleation theory provides, because the presence of these interactions invalidates some of its assumptions. In this work, we investigate the ramifications of medium-range, substrate-mediated interactions for aspects of island nucleation and growth. The interactions are quantified for Ag on a strained Ag (111) substrate using density-functional-theory calculations. We discuss our incorporation of these interactions into a kinetic Monte Carlo model to study thin-film epitaxy. The simulated thin-film growth is compared to predictions by standard nucleation theory. We discuss features of island nucleation and growth that are actuated by the presence of medium-range interactions.

PACS: 68.55.-a; 61.43.Hv; 68.35.Fx; 82.20.Mj

Achieving a quantitative understanding of the morphology that evolves when atoms are deposited onto a solid substrate is important for both fundamental and practical reasons. In the initial stages of thin-film epitaxy, before a complete layer has been deposited, atoms typically diffuse on the solid surface and aggregate to form islands. Certain aspects of island nucleation and growth appear to be common to many different systems and this has motivated the development of a theory [1, 2] to describe the salient features of the process. In a general description, gas-phase species are deposited onto an initially pristine, solid substrate with a rate F. These species diffuse on the surface with a rate $D = \nu_0 e^{-E_b^0/k_B T}$, where ν_0 is the pre-exponential factor, E_b^0 is the diffusion-energy barrier for an isolated species, k_B is Boltzmann's constant, and T is the temperature. Diffusion mediates the aggregation of adspecies into nuclei, which either dissociate if they are below a critical size, or grow subsequently to become stable islands. Initially, the formation of island nuclei is the main process taking place. As the surface coverage increases, it becomes increasingly likely that deposited species will add to stable islands and promote their growth instead of forming new nuclei. These general features can be captured in a mean-field theory for the stable island density in the island-growth regime N_x [1, 2]. In the limit of low temperatures, where all deposited atoms stick to the surface and aggregate irreversibly to form islands, this expression has the form

$$N_x \sim (F/D)^{1/3} . \quad (1)$$

The validity of (1) has been investigated experimentally in studies of several homo- and hetero-epitaxial growth systems [2–12]. Perhaps the best success of (1) is for the growth of Ag on Pt (111) [4, 5]. Using low-temperature scanning tunneling microscopy (STM), Brune et al. demonstrated that when Ag is grown on Pt (111), the island density measured at a fixed temperature scales as the deposition rate F to the $1/3$ power, as predicted by (1). Equation (1) can also be used to obtain the activation energy E_b^0 and pre-exponential factor ν_0 for adatom hopping from an Arrhenius plot of the island density as a function of temperature at a fixed deposition rate. Using this protocol in low-temperature STM studies, Brune et al. [5] found an activation energy and pre-exponential that are both consistent with values from first-principles calculations by Ratsch et al. [13, 14]. Additionally, Brune et al. [4] used kinetic Monte Carlo (kMC) simulations to model the growth of Ag on Pt (111) with the experimental parameters. In these simulations, the island density agrees well with experiment.

Barth et al. have described efforts to obtain the activation energy and the pre-exponential factor for diffusion using (1) to analyze low-temperature STM data [12]. The parameters obtained in three of these studies are shown in Table 1. A striking feature of the experimental results is that the pre-exponential factors are significantly smaller than would be anticipated for systems such as these. For example, from ab initio calculations, Ratsch and Scheffler [14] find a pre-

*Corresponding author.
(Fax: +1-814/865-7846, E-mail: fichthorn@psu.edu)

Table 1. Experimentally determined diffusion-energy barriers and pre-exponential factors using (1)

System	E_b^0 (meV)	ν_0 (s^{-1})	Ref.
Al on Au (111)	30	7×10^3	[11]
Al on Al (111)	42	8×10^6	[12]
Ag on 1-ML Ag/Pt (111)	60	10^9	[5]

exponential factor of $\nu_0 = 1.3 \times 10^{12}\,s^{-1}$ for a Ag adatom on 1-ML Ag/Pt (111), with a diffusion barrier of $E_b^0 = 63$ meV. Inserting the experimental and theoretical values for the diffusion parameters into (1), we see that the experimental island densities are about an order of magnitude higher than predictions based on the theoretical diffusion parameters. While it has been suggested that such low pre-exponential factors are, indeed, possible [12], we concluded [15] that these discrepancies indicate that the assumptions on which (1) is based are not upheld for all epitaxial growth systems – even for those that are seemingly related. In this paper, we discuss our efforts to understand the origins of the discrepancy.

We used density-functional theory (DFT) to quantify adsorbate diffusion and interactions on a strained Ag (111) surface, which we use as a model of Ag on 1-ML Ag/Pt (111) [15, 16]. We found that one of the assumptions of (1) – that interactions between adsorbed species do not extend beyond a short range – is violated. We found that, past the short range, interactions in this system are primarily pairwise and electronic in origin [15, 16] and that they form a ring-like structure around a central adatom. Similar results are found in electronic-structure calculations by Bogicevic et al. [17] for Cu adatoms on Cu (111) and for Al on Al (111).

The electronic, substrate-mediated interaction between two adsorbates is understood to arise from the electron-density perturbation that occurs when an atom binds to a surface and modifies the charge density nearby [18–21]. For the (111) surfaces of Ag, Cu, and Au, which possess Shockley-type surface states [22, 23], screening is largely mediated by the surface-state electrons, which can be approximated as a two-dimensional electron gas. In the limit that the separation d between two adsorbates is greater than the Fermi wavelength $\lambda_F = 2\pi/k_F$, the interaction energy ΔE is predicted [21] to be of the form

$$\Delta E = -A\frac{\sin(2k_F d + 2\delta)}{(k_F d)^2}, \qquad (2)$$

where A is the amplitude and δ is a phase shift, both of which depend on scattering properties of the surface-state electrons [21]. Oscillatory, ring-like, charge-density waves associated with the electronic interaction have been imaged around adatoms and defects in STM studies of the (111) surfaces of Ag, Au, and Cu [22, 24–28]. Recently, Repp et al. have quantified the pair-interaction energy for Cu atoms on Cu (111) [25]. Their studies confirm that the interaction is oscillatory with a period of $\lambda_F/2 = 15$ Å and that it decays with adsorbate separation as d^{-2}, as predicted by (2). The first (and deepest) minimum in the interaction-energy profile observed by Repp et al. [25] lies at $d = 12.5$ Å, with a depth of -0.4 meV. Beyond this distance, the interactions are weaker. For the Ag (111) surface, which has $k_F = 0.083$ Å^{-1}, the first minimum of the long-range interaction occurs at ~ 30 Å and the interactions between Co adatoms on Ag (111), probed in low-temperature STM studies by Knorr et al., are weaker than those seen for the Cu (111) surface [29].

In our studies of strained Ag (111) [15, 16], we did not probe adsorbate separations long enough for (2) to be applicable. However, substrate-mediated interactions can also occur at 'intermediate' distances less than the long separations for which (2) is applicable. For example, Einstein and Schrieffer showed in tight-binding calculations that the intermediate-range interaction is present and is more significant than the long-range interaction [19]. The experimental studies of Repp et al. also indicate that this is the case for Cu adatoms on Cu (111) [25]. At adsorbate separations slightly shorter than the first (and very weak) attractive minimum discussed above, they observed an 'extra' barrier, 15 meV above the diffusion barrier for an isolated adatom, for two Cu adatoms to aggregate to form a dimer. Thus, while the long-range interactions predicted by (2) are well understood and are very weak compared to $k_B T$ in typical growth experiments, there is evidence that the 'medium-range' interactions, which are poorly understood by comparison, can be strong enough to influence growth under experimental conditions. The electronic, pair interaction that we find for Ag on strained Ag (111) is shown in Fig. 1 for various ranked distances of an adatom from a central adatom. In Fig. 1 we see that the magnitude of the repulsive interaction at distances 11, 12, and 13 is significant and we found that it is comparable to the diffusion-energy barrier [15]. In this paper, we elaborate upon our kMC studies [15], in which we simulate thin-film epitaxy in the presence of the pair interactions shown in Fig. 1. We discuss several ramifications of these interactions for island nucleation and growth.

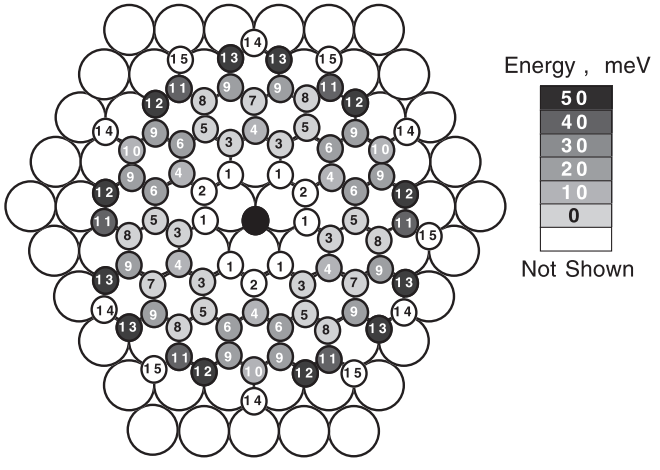

Fig. 1. Electronic pair interaction energy as a function of distance from a central adatom, shown in *black*, for Ag on strained Ag (111). The interactions at distances 1 and 2 are strongly attractive ($V^{(2)}(d=1) = -0.254$ eV, $V^{(2)}(d=2) = -0.109$ eV) and not shown. The interactions at distances 14 and 15 were not calculated for this study

1 Model and methods

Our kMC model employs the general method of Fichthorn and Weinberg [30] and incorporates the pair potential for Ag

on strained Ag (111) shown in Fig. 1. In the initial stages of thin-film epitaxy, the surface coverage is low and pair interactions are likely to be the only significant interactions governing island nucleation and growth [31, 32]. In our kMC model, atoms are deposited onto a fcc (111) substrate with a rate of $F = 0.1$ ML/s. We have also probed $F = 0.01$ ML/s. An adatom hops from site i to site j with a rate given by

$$D_{i\to j} = \nu_0 \mathrm{e}^{-E_{i\to j}/k_\mathrm{B}T}\,, \tag{3}$$

where $E_{i\to j}$ is the energy barrier to hop from site i to site j. For the pre-exponential factor, we use $\nu_0 = 10^{12}\ \mathrm{s}^{-1}$, a value consistent with results from first-principles calculations by Ratsch and Scheffler [14], who found $\nu_0 = 1.3 \times 10^{12}\ \mathrm{s}^{-1}$. The energy barrier is given by

$$E_{i\to j} = E^{\ddagger}_{i,j} - E_i\,, \tag{4}$$

where E_i is the energy with an atom at site i and $E^{\ddagger}_{i,j}$ is the energy of the transition state between site i and site j. In general, $E^{\ddagger}_{i,j}$ should depend on both E_i and E_j. Considering possible permutations of adatom configurations with 13th-neighbor interactions, a large number of different, diffusion-energy barriers could occur. To make the problem tractable, we adopt a simple model, in which

$$E_{i\to j} = E^0_\mathrm{b} + \frac{1}{2}(E_j - E_i)\,. \tag{5}$$

All of the quantities in (5) are obtained from DFT calculations. E^0_b is the diffusion-energy barrier for an isolated atom to hop from a fcc to a nearest-neighbor hcp site. We find this to be $E^0_\mathrm{b} = 52$ meV [15], in good agreement with experimental values [5] for Ag on 1-ML Ag/Pt (111) (60 meV) and with those of Ratsch and Scheffler [14] (63 meV). E_i and E_j in (5) are obtained from a sum of the pair interactions shown in Fig. 1. For example, (5) predicts that the barrier for one adatom to hop from the 14th to the 13th neighbor of a second adatom is 78 meV – a value that is 26 meV above the barrier for an isolated adatom. The simple model given by (5) upholds the detailed balance criterion. We tested (5) for a trial configuration in which an adatom with four fcc 9th neighbors hops to a nearest-neighbor hcp site where it has two 7th and two 12th neighbors. From (5), we find $E_{i\to j} = 53$ meV, which is in good agreement with the value of 46 meV from DFT calculations.

With diffusion-energy barriers of the form given by (5), there are high-energy barriers for atoms in islands to rearrange once they have aggregated. Assuming only a nearest-neighbor attraction, this would lead to fractal adsorbate islands, shaped like diffusion-limited aggregates (see, for example, [4]). In the presence of the pair interactions shown in Fig. 1, this leads to elongated, chain-like islands. Figure 2 shows the potential energy at various sites surrounding three atoms arranged in a chain vs. three atoms arranged in a triangle. In Fig. 2a we see that for a chain, the potential energies at sites at the ends of the chain are lower than the potential energies of sites that lie perpendicular to the chain axis. Thus, in the absence of rearrangement, atoms tend to add to chain ends and grow elongated islands. If three atoms can arrange in a triangle, the potential-energy landscape surrounding the island is isotropic, as shown in Fig. 2b. The kinetics

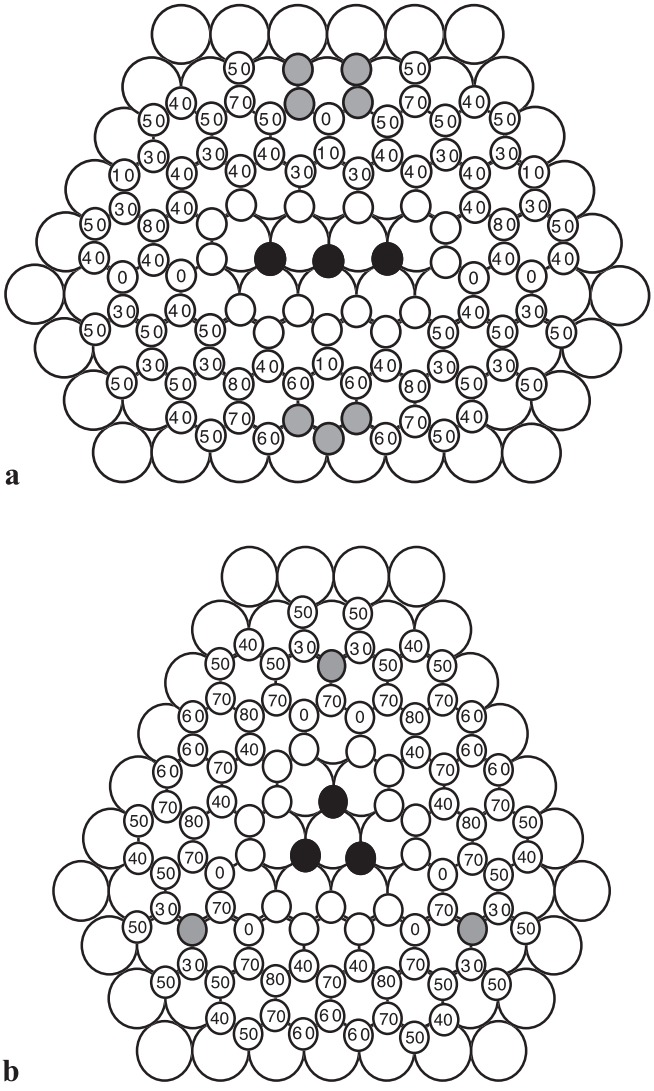

Fig. 2a,b. Interaction energies (in meV) at various binding sites surrounding a three-atom island with the atoms arranged in a chain (**a**) and in a triangle (**b**). Sites for which the interaction energy is greater than 100 meV are *highlighted*. The energies for sites with attraction are not indicated

of island rearrangement determines whether islands remain compact or assume an elongated form. Experimental STM images of islands formed during the deposition of Ag on 1-ML Ag/Pt (111) indicate that the Ag islands do not form long, single-atom chains [2, 5].

Theoretical studies of adatom diffusion along close-packed step edges indicate that energy barriers for this process are typically lower than energy barriers for diffusion on terraces [33–35], and that adatom hopping along steps may occur via concerted processes [33, 37]. Theoretical studies using semi-empirical potentials show that the kinetics of small-island motion and rearrangement can involve complicated, many-atom processes [36, 37]. To mimic these features, we adopt a simple model to allow for island rearrangement. In our model, we allow an fcc (hcp) atom with one or more nearest neighbors to hop to a nearest-neighbor fcc (hcp) site (i.e. distance 1 in Fig. 1) and, thus, avoid the intermediate hcp (fcc) site. These hops occur in addition to hops between neighboring fcc and hcp sites. The energy barriers for these longer hops are of the form given

by (5) with E_b^0 equal to a value 1.5–2.0 times higher than the hopping barrier for an isolated atom. In this way, we achieve compact islands. Although our diffusion model satisfies the detailed-balance criterion, and should produce correct island shapes at equilibrium, this model does not ensure that we will achieve correct *kinetic* island shapes away from equilibrium.

Brune et al. used kMC simulations to study the influence of island-edge mobility on the island density in a model of Ag deposition on Pt (111) [4]. By varying this mobility, they achieved island shapes ranging from fractal (diffusion-limited aggregates) to dendritic to compact. In all cases, (1) is satisfied and the proportionality coefficient η needed to set the magnitude of the island density (i.e. $N_x = \eta \times (F/D)^{1/3}$) varies between 0.2 and 0.23. These values are in good agreement with the theoretical estimate by Bales and Chrzan [38] of $\eta = 0.25$. Thus, it appears that the island density, at least that for compact or semi-compact, isotropic islands, is not very sensitive to island shape and our procedure for achieving compact islands should have little or no impact on the simulated island density.

We used our kMC model (denoted as the DFT-kMC model) to simulate thin-film epitaxy over temperatures ranging between 40 and 70 K and we determined island densities in the island-growth regime. These low temperatures are in the range of the experimental studies (cf. Table 1). To put our results in context and to better understand them, we ran simulations using a caricature model, which we denote as the repulsive-ring model. In this model, we replace the set of pair interactions shown in Fig. 1 with the nearest-neighbor attractive interaction and a uniform, repulsive ring of strength ε_R at distances 10–13 in Fig. 1. Interactions at all other distances are set to zero. By varying the magnitude of ε_R, we span the entire range of possible behaviors in this system. One limit of interest is when $\varepsilon_R = 0$ and we only have nearest-neighbor attraction. By suppressing long-range interactions, we create a model that is consistent with the assumptions behind (1). Results from these simulations allow us to quantify the extent to which the interactions in Fig. 1 influence the island density and the extent to which experiments using (1) will be in error when the assumptions of this theory are violated.

2 Results

Figure 3 shows an Arrhenius plot of the island density from our DFT-kMC model as a function of temperature for a deposition rate of $F = 0.1$ ML/s. Also shown in Fig. 3 is the island density predicted by (1) for the values of F, ν_0, and E_b^0 used here. As discussed above, a proportionality coefficient η is needed to quantitatively compare nucleation theory with the simulations. We use the theoretical estimate by Bales and Chrzan [38] of $\eta = 0.25$. In Fig. 3, we see that the DFT-kMC island densities are an order of magnitude (or more) above the values predicted by (1). Returning to our discussion of the experimental results shown in Table 1, we point out that the order-of-magnitude difference between the island densities predicted from ab initio calculations [14] and those found experimentally for Ag on 1-ML Ag/Pt (111) [5] is also seen in our study, comparing the island densities predicted by nucleation theory to those found in our DFT-kMC 'computer experiments' (cf. Fig. 3). Thus, we conclude that our results can explain the theoretical–experimental gap in the island density for Ag on 1-ML Ag/Pt (111).

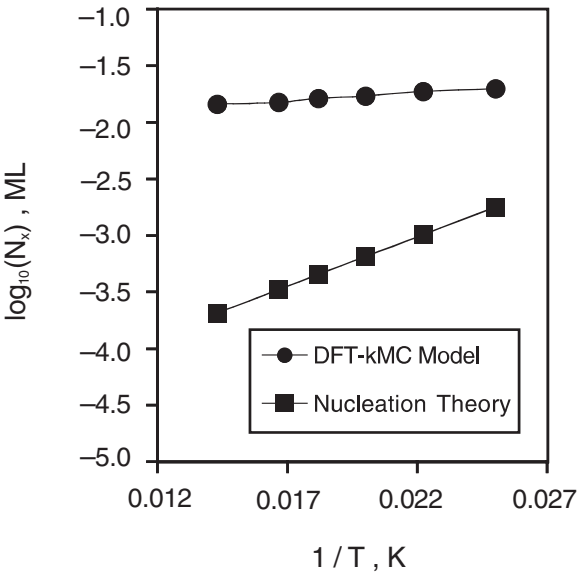

Fig. 3. Arrhenius plot of the island density (in ML) as a function of temperature (in K) for the DFT-kMC model with $F = 0.1$ (*circles*) compared to the prediction from (1) (*squares*). The *lines* with the DFT-kMC results are to guide the eye

The repulsive-ring model allows us to study the features contributing to the high island density and to test the sensitivity of the results to the magnitude of the interactions. In Fig. 4 we show results from the repulsive-ring model along with the DFT-kMC results and predictions from nucleation theory. We see that we can fit the DFT-kMC results with $\varepsilon_R = 50$ meV.

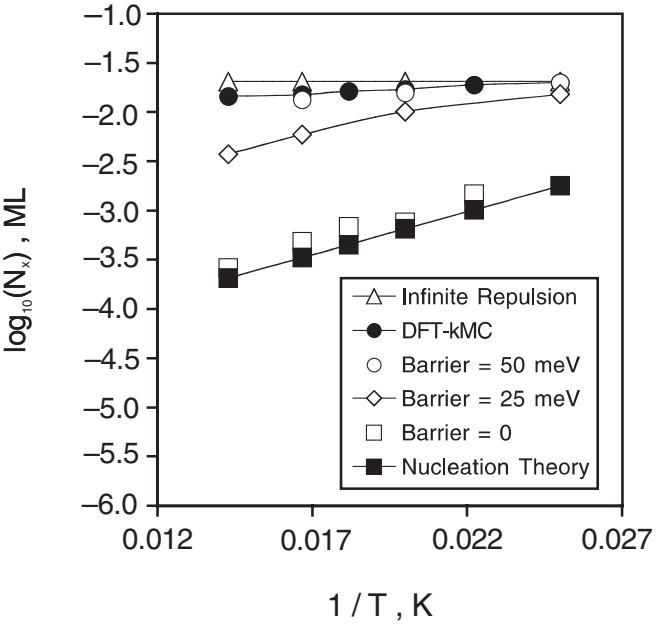

Fig. 4. Arrhenius plot of the island density as a function of temperature from an impermeable repulsive ring (*open triangles*), the DFT-kMC model (*closed circles*), a repulsive ring with $\varepsilon_R = 50$ meV (*open circles*), a repulsive ring with $\varepsilon_R = 25$ meV (*diamonds*), a repulsive ring with $\varepsilon_R = 0$ (*open squares*), and (1) (*closed squares*). The *lines* are to guide the eye

Also, for $\varepsilon_R = 0$, we recover the results predicted by (1) – although our simulations suggest that the proportionality constant η described above should be slightly higher than 0.25. As $\varepsilon_R \to \infty$, the island density assumes a constant, maximum value that is independent of temperature (cf. Fig. 4). This is because island nucleation can only occur when one atom is deposited within the repulsive ring of another and it is governed by the temperature-independent deposition rate. In this regime, many adatoms are isolated by repulsion in the initial stages of deposition. Each isolated adatom becomes a stable island when another atom is deposited into its ring and the resulting island density is significantly higher than in the absence of such a ring.

As ε_R is decreased, diffusing adatoms are increasingly able to surmount the ring barrier and a second channel for island nucleation and growth (via long-range, adatom diffusion) opens up. The extent to which long-range diffusion contributes to island nucleation and growth depends on the temperature. In Fig. 4 we see that at 40 K the DFT-kMC island density is the same as that for an infinitely repulsive ring. As the temperature increases, adatoms are increasingly able to penetrate the ring barrier to aggregate and add to existing islands via long-range diffusion. Consequently, the island density decreases with increasing temperature. It is interesting to note that for the conditions studied, even a repulsive ring with $\varepsilon_R = 25$ meV – half the magnitude found in our DFT calculations – can lead to significantly higher island densities than those predicted by nucleation theory.

Analysis of the island density shows only part of the complex process of island formation and growth in the presence of long-range interactions. More insight into this process can be gained by inspecting the morphology of the films. In Fig. 5 we show a snapshot from a DFT-kMC simulation at 50 K and a fractional coverage $\theta \sim 0.024$. We also show a map of the potential energy of a test particle that was placed in vacant lattice sites. The potential energy is obtained from a sum of the pair interactions from the pair potential shown in Fig. 1 and the potential-energy map shows the repulsive rings surrounding adatoms and islands. One interesting feature of this plot is that, even at this very low coverage, almost all of the atoms have aggregated into islands and only three, single adatoms can be seen. This percentage is in sharp contrast to what is seen at the same temperature and coverage in the repulsive-ring model with $\varepsilon_R \to \infty$, where $\sim 60\%$ of the deposited atoms remain single. Thus, even though the steady-state island densities are nearly the same for the infinitely repulsive ring and the DFT-kMC model at 50 K (cf. Fig. 3), the film morphologies are different.

From comparing the potential energies around a single atom to those around islands with two, three, and four atoms, we see in Fig. 5 that the repulsion surrounding an island increases with increasing island size. This can be seen for compact islands, as the potential energy in the surrounding ring moves to darker shades on the scale. For a single atom, the repulsion is typically 50 meV (cf. Fig. 1). In Fig. 2 we see that, for trimers, the surrounding potential energy has increased to typically 60–70 meV. These observations suggest that at a fixed temperature, small, stable islands form rapidly on the time scale of deposition and grow to a size determined by a 'growth barrier' that arises from pairwise interactions of an adatom with island atoms. Subsequently, these islands grow when adatoms hop over the growth barrier or when adatoms are deposited within growth-barrier regions. As we see in Fig. 5, these regions exist within the repulsive rings surrounding isolated islands or within the 'repulsive-ridge' areas that form between adjacent islands. When an adatom is deposited onto the repulsive-ridge area between islands, it can be funneled down the potential-energy gradient to add to another atom or to an existing island. As the surface coverage increases, it becomes increasingly likely that atoms will be deposited within the growth-barrier regions. Figure 6 shows the island structure along with a potential-energy map for a DFT-kMC simulation run at 50 K at a coverage of $\theta = 0.15$. At this coverage, the system has reached the island-growth regime, where the island density remains nearly constant over time until island coalescence begins to occur frequently and the island density decreases. In Fig. 6 we see that most of the vacant sites where an adatom would be deposited lie in the 'repulsive-ridge' area between islands. There are only a few, small pockets of low potential energy, where deposited atoms would most likely be trapped by the surrounding repulsion and would be unlikely to add to existing islands.

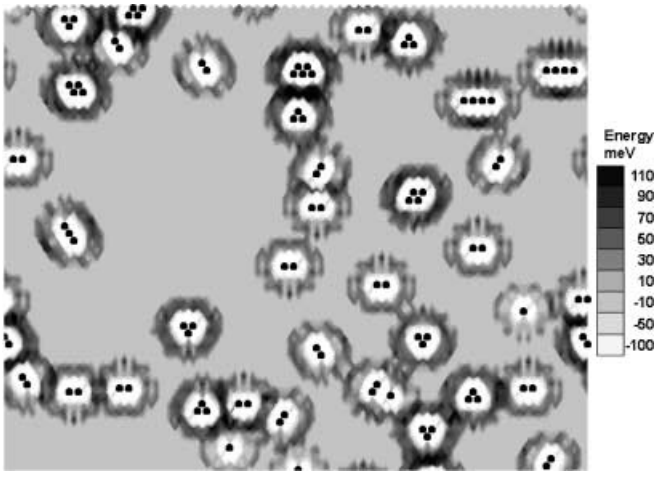

Fig. 5. Simulated DFT-kMC film morphology at 50 K and $\theta = 0.024$ along with a map of the potential energies in vacant sites

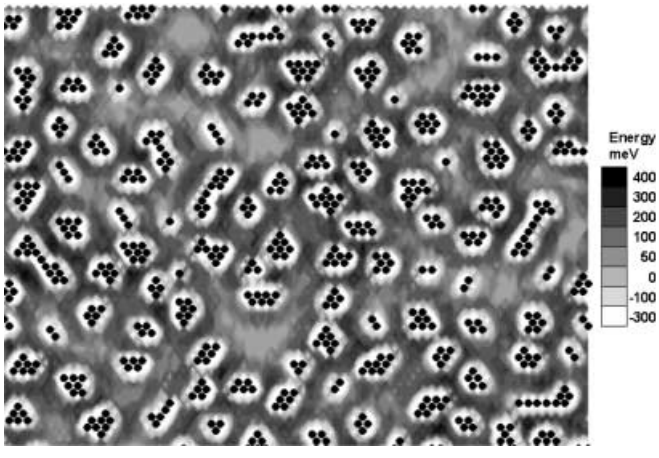

Fig. 6. Simulated DFT-kMC film morphology at 50 K and $\theta = 0.15$ along with a map of the potential energies in vacant sites

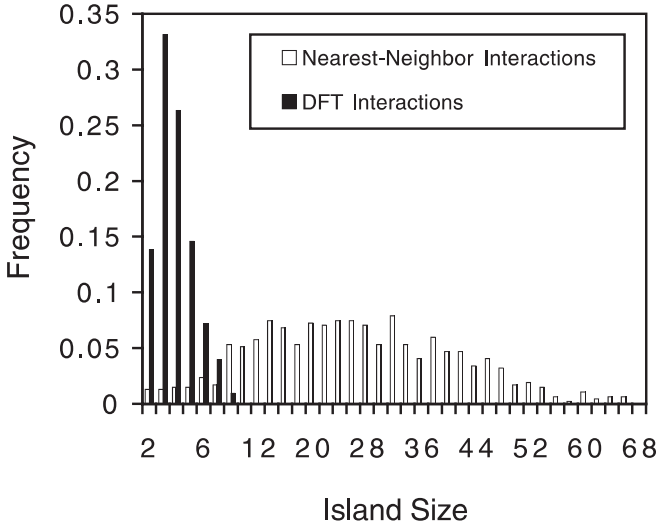

Fig. 7. Island-size distributions at $F = 0.01$ ML/s from the DFT-kMC model and from the repulsive-ring model with $\varepsilon_R = 0$ at 35 K. The fractional coverage is $\theta = 0.07$

The existence of island-size-dependent growth barriers should have ramifications for the island-size distribution. Here, we report some preliminary results with $F = 0.01$ ML/s in which we obtained island-size distributions at a coverage of $\theta = 0.07$ – in the middle of the island-nucleation regime. The island-size distribution is dependent on coverage and it broadens slightly toward larger island sizes as the coverage increases through the island-nucleation regime. We find that the island-size distribution can be considerably sharper in the presence of a repulsive ring than for the nearest-neighbor interactions assumed by (1). For example, Fig. 7 shows that, at 35 K, the island-size distribution in the presence of a repulsive ring is about an order of magnitude sharper than with nearest-neighbor interactions. In the presence of the repulsive ring, about 70% of the islands are either dimers or trimers. The existence of size-dependent growth barriers provides an extra degree of freedom for engineering nanostructures at surfaces. Future theoretical and experimental studies in this area would be beneficial.

3 Discussion and conclusions

We presented some of the ramifications of medium-range, substrate-mediated interactions for island nucleation and growth in thin-film epitaxy. The pair interactions are quantified for Ag on a strained Ag (111) substrate using DFT [15] and they lead to the formation of a repulsive ring around individual atoms. Experimental evidence [25] for the existence of such a ring exists for Cu on Cu (111), which has an electronic structure similar to that of Ag (111). Using kMC simulations, we find that these interactions lead to island densities substantially larger than those predicted by standard nucleation theory. The existence of repulsive interactions can inhibit island nucleation. However, at the temperatures and deposition rates probed here, island nucleation occurs on the time scale of deposition – as evidenced by the near absence of adatoms in simulated films at low temperatures and coverages. We conclude that repulsive, substrate-mediated interactions primarily inhibit island growth in our simulations. Analysis of potential-energy maps of binding sites surrounding deposited atoms and islands reveals that repulsive 'growth barriers' form around small islands. Because of the pair-wise additivity of the substrate-mediated interaction, these growth barriers are larger than the repulsion surrounding a single adatom and they increase with increasing island size. This suggests a picture in which nearly monodisperse islands form early in the deposition process. As more atoms are deposited, the number of these islands increases until the repulsive growth barriers surrounding them begin to overlap, and it is more likely that adatoms will be deposited in the overlap region than in low potential energy regions that are isolated from other islands. The existence of substrate-mediated interactions should be considered in attempts to engineer nanostructures at surfaces, and future theoretical and experimental investigations would be fruitful.

Acknowledgements. Support for this work is from the Alexander von Humboldt Foundation and the NSF (DMR-9617122, DGE-9987589, and EEC-0085604).

References

1. J.A. Venables: Philos. Mag. **27**, 697 (1973)
2. H. Brune: Surf. Sci. Rep. **31**, 121 (1998)
3. J.A. Stroscio, D.T. Pierce, R.A. Dragoset: Phys. Rev. Lett. **70**, 3615 (1993)
4. H. Brune, G.S. Bales, J. Jacobsen, C. Boragno, K. Kern: Phys. Rev. B **60**, 5991 (1999)
5. H. Brune, K. Bromann, H. Röder, K. Kern, J. Jacobsen, P. Stoltze, K. Jacobsen, J. Norskov: Phys. Rev. B **52**, R14 380 (1995)
6. B. Müller, B. Fischer, L. Nedelmann, H. Brune, K. Kern: Phys. Rev. B **54**, 17 858 (1996)
7. M. Bott, M. Hohage, M. Morgenstern, T. Michely, G. Comsa: Phys. Rev. Lett. **76**, 1304 (1996)
8. J.K. Zuo, J.F. Wendelken, H. Dürr, C.L. Liu: Phys. Rev. Lett. **72**, 3064 (1994)
9. C.-M. Zhang, M.C. Bartelt, J.-M. Wen, J.W. Evans, P.A. Thiel: J. Cryst. Growth **174**, 851 (1997)
10. S. Günther, E. Kopatzki, M.C. Bartelt, J.W. Evans, R.J. Behm: Phys. Rev. Lett. **73**, 553 (1994)
11. B. Fischer, H. Brune, J.V. Barth, A. Fricke, K. Kern: Phys. Rev. Lett. **82**, 1732 (1999)
12. J.V. Barth, H. Brune, B. Fischer, J. Weckesser, K. Kern: Phys. Rev. Lett. **84**, 1732 (2000)
13. C. Ratsch, A.P. Seitsonen, M. Scheffler: Phys. Rev. B **55**, 6750 (1997)
14. C. Ratsch, M. Scheffler: Phys. Rev. B **58**, 13 163 (1998)
15. K.A. Fichthorn, M. Scheffler: Phys. Rev. Lett. **84**, 5371 (2000)
16. K.A. Fichthorn, M. Scheffler: In *Collective Diffusion on Surfaces: Collective Behavior and the Role of Adatom Interactions*, ed. by M.C. Tringides, Z. Chvoj (Kluwer, Dordrecht 2001) p. 225
17. A. Bogicevic, S. Ovesson, P. Hyldgaard, B.I. Lundqvist, H. Brune, D.R. Jennison: Phys. Rev. Lett. **85**, 1910 (2000)
18. K.H. Lau, W. Kohn: Surf. Sci. **75**, 69 (1978)
19. T.L. Einstein, J.R. Schrieffer: Phys. Rev. B **7**, 3629 (1973)
20. T.L. Einstein: *Handbook of Surface Science*, Vol. 1, ed. by W.N. Unertl (Elsevier, Amsterdam 1996) p. 577
21. P. Hyldgaard, M. Persson: J. Phys.: Condens. Matter **12**, L13 (2000)
22. O. Jeandupeux, L. Burgi, A. Hirstein, H. Brune, K. Kern: Phys. Rev. B **59**, 15 926 (1999)
23. S.D. Kevan, R.H. Gaylord: Phys. Rev. B **36**, 5809 (1987)
24. B.G. Briner, Ph. Hoffman, M. Döring, H.-P. Rust, A.M. Bradshaw, L. Petersen, P.T. Sprunger, E. Laegsgaard, F. Besenbacher, E.W. Plummer: Europhys. News **28**, 148 (1997)

25. J. Repp, F. Moresco, G. Meyer, K.-H. Rieder: Phys. Rev. Lett. **85**, 2981 (2000)
26. P. Avouris, I.W. Lyo, P. Molinasmata: Chem. Phys. Lett. **240**, 423 (1995)
27. M.F. Crommie, C.P. Lutz, D.M. Eigler: Nature **363**, 524 (1993)
28. E.J. Heller, M.F. Crommie, C.P. Lutz, D.M. Eigler: Nature **369**, 464 (1994)
29. N. Knorr, H. Brune, M. Epple, A. Hirstein, M.A. Schneider, K. Kern: Phys. Rev. B **65**, 115420 (2002)
30. K.A. Fichthorn, W.H. Weinberg: J. Chem. Phys. **95**, 1090 (1991)
31. We find that trio interactions are unimportant at the medium and longer distances shown in Fig. 1 and we will discuss them elsewhere
32. T.L. Einstein: Surf. Sci. **84**, L497 (1979)
33. P. Ruggerone, C. Ratsch, M. Scheffler: In *The Chemical Physics of Solid Surfaces*, Vol. 8, eds. by D.A. King, D.P. Woodruff (Elsevier, Amsterdam 1997) p. 490
34. S. Ovesson, A. Bogicevic, B.I. Lundqvist: Phys. Rev. Lett. **83**, 2608 (1999)
35. B.-D. Yu, M. Scheffler: Phys. Rev. B **55**, 13916 (1997)
36. G. Henkelman, G. Jóhannesson, H. Jónsson: In *Progress on Theoretical Chemistry and Physics*, ed. by S.D. Schwartz (Kluwer, Dordrecht 2000)
37. A.L. Miron, K.A. Fichthorn: J. Chem. Phys. **115**, 8742 (2001)
38. G.S. Bales, D.C. Chrzan: Phys. Rev. B **50**, 6057 (1994)